A SEAMLESS HYBRID RANS–LES MODEL BASED ON TRANSPORT EQUATIONS FOR THE SUBGRID STRESSES AND ELLIPTIC BLENDING

Atabak Fadai-Ghotbi, Rémi Manceau & Jacques Borée
Laboratoire d'Etudes Aérodynamiques
UMR 6609 CNRS/Université de Poitiers/ENSMA
SP2MI, Bd. Curie, BP 30179, 86962 Futuroscope Chasseneuil Cedex, France
remi.manceau@lea.univ-poitiers.fr

Keywords: Partially-integrated Transport Model ; Near-wall Turbulence; Elliptic relaxation ; Channel Flow; Spectral Theory of Turbulence; Dissipation Equation.

ABSTRACT

The aim of the present work is to develop a seamless hybrid RANS–LES model, using the elliptic blending method to account for the kinematic wall blocking effect. In order to reproduce the complex production and redistribution mechanisms when the cutoff wavenumber is located in the productive region of the turbulent spectrum, the model is based on transport equations for the subgrid stress tensor. The PITM (Partially Integrated Transport Model) methodology offers a consistent theoretical framework for such a model, enabling to control the cutoff wavenumber κ_c, and then the transition from RANS to LES, by making the C_{ε_2} coefficient in the dissipation equation of a RANS model a function of κ_c. The extension of the underlying RANS model used in the present work, the elliptic blending Reynolds-stress model (EB-RSM), to the hybrid RANS–LES context, brings out some modelling issues which are discussed in the paper. The different modelling possibilities are tested in a channel flow at $Re_\tau = 395$. The final model gives encouraging turbulent statistics. In particular, the anisotropy of turbulence in the near-wall region is satisfactorily reproduced, although it is far from perfectly matching the DNS results. The contribution of the resolved and modelled part to the Reynolds stresses behaves as expected: the modelled part is dominant in the near-wall zone (RANS mode) and decreases toward the centre of the channel, where the resolved part in turn becomes dominant (LES mode). Moreover, when the mesh is refined, more energy is resolved, but the total Reynolds stresses remain approximately constant. The mean velocity profile is satisfactorily reproduced and weakly dependant of the mesh, contrary to what is observed in LES with a dynamic Smagorinsky model.

INTRODUCTION

Problems ranging from noise prediction to fluid/structure interaction or thermal fatigue require the computation of time-dependent characteristics of complex flows. RANS (*Reynolds-Averaged Navier-Stokes*) computations are often used in industrial configurations because they are cheap, their cost being weakly dependent on the Reynolds number, and the mean flow and the turbulence statistics can be predicted with accuracy in attached flows. But RANS calculations are not able to provide unsteady information because all the turbulent scales are modelled. On the contrary, LES (*Large Eddy Simulation*) can provide the necessary information by resolving the large-scale structures, and modelling the smaller scales. However, at high Reynolds numbers, LES is considered too CPU-demanding for complex industrial applications. One reason is that the cutoff wavenumber, separating resolved and modelled scales, must be located in the inertial part of the turbulence spectrum, leading to the use of fine meshes. In particular, a limitation of LES is the resolution required for the crucial near-wall regions, which is to be solved in a Q-DNS mode (*Quasi-Direct Numerical Simulation*), in order to avoid the use of wall function.

Therefore, a wide variety of relatively low-cost strategies (compared to LES) have recently emerged for performing unsteady computations: VLES (*Very Large Eddy Simulation*) [22], LNS (*Limited Numerical Scales*) [2], DES (*Detached Eddy Simulation*) [21], URANS (*Unsteady Reynolds-Averaged Navier-Stokes*) [13], OES (*Organized Eddy Simulation*) [12], SAS (*Scale-Adaptive Simulation*) [16], PANS (*Partially-Averaged Navier-Stokes*) [11], PITM (*Partially Integrated Transport Model*) [19], among others. Computations based on a RANS model in some regions of the flow, in particular in the near-wall regions, and on LES in some other regions, where explicit computation of the large-scale structures is required, are referred to as *hybrid RANS-LES* computations. When the transition RANS→LES occurs in a continuous manner, the model is said to be *seamless*, meaning that there is no need to define explicit frontiers between RANS and LES regions. In homogeneous flows, this type of models can be seen as a LES with a cutoff wavenumber κ_c continuously going to zero, or, equivalently, as a LES with a filter width continuously going to infinity (spatial average).

Using such a model, between a RANS region and the LES region, there is necessarily, by continuity, a region (called the *grey zone* in DES), where the cutoff wavenumber is located in the energetic part of the spectrum. The challenge is thus to be able to reproduce the complex production and redistribution mechanisms which occur at these scales, which are very difficult, if not impossible at all, to be accounted for using an algebraic relation between the subgrid stress and the resolved velocity gradients. Moreover, when the cutoff is located in the energy containing region, the knowledge of the subgrid-scale kinetic energy is necessary to reconstruct the total Reynolds stresses. Therefore, in the present paper, a model based on transport equations for the subgrid stress tensor is developed. This better representation of the physical mechanisms is at the price of an increase of the CPU cost, but one of the purposes of using such a model is to enable the use of coarser meshes than in a classical LES, which requires a cutoff wavenumber in the inertial region: a slight coarsening of the mesh can by far compensate for the cost of solving additional transport equations. Another challenge is to provide a theoretical framework to the separation resolved/modelled scales which bridges RANS and LES. Recently, such a theoretical framework has been proposed [19], the so-called PITM, and used with transport equations for the subgrid-stress tensor and the dissipation rate [4]. As a result of modelling in spectral space, with a variable cutoff wave-number κ_c, compatibility is guaranteed with the two extreme limits that are RANS ($\kappa_c \to 0$) and DNS ($\kappa_c \to \infty$).

The originality of the present work is the use of transport equations for the subgrid-scale stresses based on the application of the elliptic blending strategy to reproduce the non-viscous, non-local blocking effect of the wall. The present model is indeed an adaptation to the hybrid RANS-LES approach of the *Elliptic Blending Reynolds Stress Model* (EB-RSM) [15, 14], which is a near-wall extension of the SSG model [23], using the elliptic relaxation strategy of Durbin [8]. This model was successfully applied to different configurations in a RANS methodology [14, 24, 3, 25, 20, 5].

The aim of the present paper is thus to adapt the elliptic blending model to the hybrid context, using PITM approach. Modelling issues are presented and discussed. The new model is derived and calibrated in a channel flow at $Re_\tau = 395$, in comparison against DNS data [17].

GOVERNING EQUATIONS

The instantaneous flow is driven by the incompressible Navier-Stokes equations. The instantaneous velocity U_i^* is decomposed into a resolved part $\tilde{U}_i$, including mean value and large-scale fluctuations, and a residual fluctuating part u_i'' such that

$$U_i^* = \tilde{U}_i + u_i''. \quad (1)$$

The resolved velocity is obtained by the convolution product of a filter G with the instantaneous velocity as

$$\tilde{U}_i(\mathbf{x},t) = \langle U_i^* \rangle = \int_{\mathcal{D}} G(\mathbf{x}-\mathbf{r}) U_i^*(\mathbf{r},t)\,\mathrm{d}\mathbf{r}, \quad (2)$$

where $\mathcal{D}$ is the fluid domain The long-time average of U_i^* is denoted by U_i, so that the large-scale fluctuation is $u_i' = \tilde{U}_i - U_i$, and the total fluctuation is $u_i = U_i^* - U_i = u_i' + u_i''$. In the filtered Navier-Stokes equations, the subgrid-scale (SGS) tensor τ_{ij} appears, which is the tensor of the generalized central moments $\tau_{ij} = \tau(U_i^*, U_j^*)$ defined by $\tau(f,g) = \langle fg \rangle - \langle f \rangle \langle g \rangle$. The exact transport equation for τ_{ij} is given by Germano [9]

$$\frac{\tilde{D}\tau_{ij}}{\tilde{D}t} = \underbrace{-\frac{\partial \tau(U_i^*, U_j^*, U_k^*)}{\partial x_k}}_{D_{ij}^T} + \underbrace{\nu \frac{\partial^2 \tau_{ij}}{\partial x_k \partial x_k}}_{D_{ij}^\nu} \underbrace{- 2\nu\tau\left(\frac{\partial U_i^*}{\partial x_k}, \frac{\partial U_j^*}{\partial x_k}\right)}_{\varepsilon_{ij}}$$
$$\underbrace{-\frac{1}{\rho}\tau\left(U_i^*, \frac{\partial P^*}{\partial x_j}\right) - \frac{1}{\rho}\tau\left(U_j^*, \frac{\partial P^*}{\partial x_i}\right)}_{\phi_{ij}} \underbrace{-\tau_{ik}\frac{\partial \tilde{U}_j}{\partial x_k} - \tau_{jk}\frac{\partial \tilde{U}_i}{\partial x_k}}_{P_{ij}}, \quad (3)$$

where $\tilde{D}/\tilde{D}t = \partial_t + \tilde{U}_k \partial_k$, and $\tau(f,g,h) = \langle fgh \rangle - \langle f \rangle \tau(g,h) - \langle g \rangle \tau(h,f) - \langle h \rangle \tau(f,g) - \langle f \rangle \langle g \rangle \langle h \rangle$. The subgrid stress production P_{ij} and the viscous diffusion D_{ij}^ν are exact terms and need not to be modelled. The turbulent diffusion by the subgrid scales D_{ij}^T is modelled by a generalized gradient hypothesis [6]. The most crucial term to be modelled in Eq. (3) is the velocity–pressure gradient correlation (hereafter the *pressure term*) ϕ_{ij}. An adaptation of the EB-RSM model [14], usually applied in the RANS context, is used. The model blends the "homogeneous" (away from the wall) and the near-wall models of the pressure term ϕ_{ij} and the dissipation tensor ε_{ij} using

$$\phi_{ij} = (1-\alpha^2)\phi_{ij}^w + \alpha^2 \phi_{ij}^h, \quad (4)$$

$$\varepsilon_{ij} = (1-\alpha^2)\frac{\tau_{ij}}{k_m}\varepsilon + \alpha^2 \frac{2}{3}\varepsilon\delta_{ij}, \quad (5)$$

where $k_m = \frac{1}{2}\tau_{ii}$ is the modelled fluctuating kinetic energy and α is a blending coefficient which goes from zero at the wall, to unity far from the wall. Following the elliptic relaxation strategy of Durbin [7, 8], an elliptic, linear differential equation for α is proposed to reproduce the non-local blocking effect of the wall

$$\alpha - L_{\text{SGS}} \nabla^2 \alpha = 1. \quad (6)$$

As shown by [14], the correct form of ϕ_{ij}^w can be obtained by an analysis of the asymptotic behaviours at the wall, which gives

$$\phi_{ij}^w = -5\frac{\varepsilon}{k_m}\left[\tau_{ik}n_j n_k + \tau_{jk}n_i n_k - \frac{1}{2}\tau_{kl}n_k n_l\left(n_i n_j + \delta_{ij}\right)\right], \quad (7)$$

where $\mathbf{n} = \boldsymbol{\nabla}\alpha / \|\boldsymbol{\nabla}\alpha\|$ is a generalized wall-normal vector.

The Speziale, Sarkar and Gatski (SSG) model [23] is used for ϕ_{ij}^h. The modelled transport equation for the energy dissipation rate $\varepsilon = \varepsilon_{ii}/2$ is written in the same form as in the case of the RANS context

$$\frac{\tilde{D}\varepsilon}{\tilde{D}t} = C_{\varepsilon_1}\frac{P}{T} - C_{\varepsilon_2}^*\frac{\varepsilon}{T} + \frac{\partial}{\partial x_l}\left(\nu\delta_{lm} + C_s T \tau_{lm}\right)\frac{\partial \varepsilon}{\partial x_m}, \quad (8)$$

with $P = P_{kk}/2$, but following the PITM methodology [4, 19], the coefficient $C_{\varepsilon_2}^*$ is made dependant on the filter by using

$$C_{\varepsilon_2}^* = C_{\varepsilon_1} + f_k(C_{\varepsilon_2} - C_{\varepsilon_1}) \quad (9)$$

where $f_k = \overline{k_m}/k$ and $k = k_r + \overline{k_m}$ is the total turbulent energy, sum of the resolved part $k_r = \frac{1}{2}(\overline{\tilde{U}_i\tilde{U}_i} - U_i U_i)$ and modelled part $\overline{k_m} = \frac{1}{2}\overline{\tau_{ii}}$, the over-bar denoting the long-time average. The parameter f_k depends on the cutoff wavenumber and controls the transition from a RANS behaviour, where all the turbulent scales are modelled ($f_k = 1$), to a DNS behaviour, where all turbulent scales are resolved ($f_k = 0$). A relation between this parameter and the cutoff wavenumber is required and will be discussed in the next section. The time scale appearing in Eq. (8) is the subgrid time scale k_m/ε bounded by the Kolmogorov scale to avoid singularities at the walls [14]. The advantages of the elliptic blending strategy are the following:

- Unlike classical near-wall models, the EB-RSM does not make use of any damping functions or wall-echo terms to reproduce the wall effects.
- The model is derived from the Poisson equation for pressure fluctuations and asymptotic behaviours of the pressure term in the vicinity of the wall, which are both formally identical in the RANS context (statistical averaging) and the LES context (filtering).
- There is no explicit dependence on the distance to the wall, and therefore the model can be used in complex geometries.
- The elliptic blending model is much more robust than other models based on elliptic relaxation and also less CPU-demanding since a single additional equation (Eq. 6) is to be solved.

MODELLING ISSUES

As mentioned before, some modelling issues remain and must be discussed. Some of them are related to the PITM methodology and others are due to the development of an elliptic blending model in the hybrid context:

- The value of the parameter f_k must be chosen such a way that it is consistent with the two limits that are RANS ($f_k = 1$) and DNS ($f_k = 0$).

- The elliptic equation Eq. (6) enables to account for the non-local blocking effect of the wall on the subgrid stress. This effect reflects the incompressibility condition for the non-resolved scales. In a hybrid context, the blocking of the large scales, which are explicitly resolved, follows from the explicit resolution of the continuity equation ($\partial_k \tilde{U}_k = 0$). The elliptic blending aims at imposing the blocking effect only on the modelled scales, which implies that the correlation length scale L_{SGS}, entering Eq. (6), must be decreased compared to the RANS case, where all the scales of motion are modelled.

- It is usual to assume that the small scales return to isotropy faster than the large scales, which could be reproduced, as suggested by [4], by making the slow part of the pressure term a function of the width of the filter.

NUMERICAL METHOD

To investigate the previous issues, the test case of a channel flow at $Re_\tau = u_\tau H/(2\nu) = 395$ is considered, where H is the channel width and u_τ the friction velocity. Computations are performed with *Code_Saturne*, a parallel, finite volume solver on unstructured grids, developed at EDF [1]. Space discretization is based on a collocation of all the variables at the centre of gravity of the cells. Velocity/pressure coupling is ensured by the SIMPLEC algorithm, with a Rhie & Chow interpolation in the pressure-correction step. The Poisson equation is solved with a conjugate gradient method. Time advancement is based on a Crank-Nicolson scheme. Spatial derivatives are approximated by a second-order central-difference scheme (CDS) for the resolved velocity field and a first-order upwind-difference scheme (UDS) for the subgrid turbulence field. Two meshes are used, whose characteristics are given in Tab. 1. The first point near the wall is placed at $y_1^+ = 1.5$. The mesh is uniform in the homogeneous directions, in which periodic conditions are imposed. Due to the rapid variations in space and time of the filtered field, it was found necessary to average the strain tensor in the homogeneous directions before evaluating the source terms of the subgrid-stress transport equations to avoid relaminarization, a practice similar to what is done for the Smagorinsky coefficient in the dynamic procedure in LES.

Mesh	N_x	N_y	N_z	Δx^+	Δy_c^+	Δz^+
1	32	54	32	100	40	50
2	64	70	64	50	28	25

Table 1: Meshes characteristics. N_x, N_y and N_z denote the number of points in the streamwise, wall normal and spanwise directions respectively. The subscript c refers to the centre of the channel.

MODELLING OF THE PARAMETER F_K

As proposed by [19] and [4], using a Kolmogorov energy spectrum, it can be shown that the parameter f_k can be linked to the cutoff wave-number by

$$f_k = \frac{3C_K}{2}\left(\kappa_c \frac{k^{3/2}}{\varepsilon}\right)^{-2/3} \quad \text{where} \quad \kappa_c = \frac{2\pi}{C_g \Delta}, \qquad (10)$$

with $\Delta = (\Delta x \Delta y \Delta z)^{1/3}$, $C_K \simeq 1.5$ the Kolmogorov constant, and C_g a constant depending on the numerical schemes and necessarily greater than 2 to satisfy the Shannon constraint. Eq. (10) is compatible with the DNS limit ($\lim_{\kappa_c \to \infty} f_k = 0$) but not with the RANS limit ($\lim_{\kappa_c \to 0} f_k = 1$), simply because the Kolmogorov $-5/3$ power law is not valid at large scales. [4, 19] proposed the empirical modification

$$f_k = \frac{1}{1 + \beta_0 \eta_c^{2/3}} \quad \text{where} \quad \eta_c = \frac{\pi}{\Delta}\frac{k^{3/2}}{\varepsilon}, \qquad (11)$$

with $\beta_0 = \frac{2}{3C_K}\left(\frac{2}{C_g}\right)^{2/3} \leq 0.44$. The integral length scale $k^{3/2}/\varepsilon$ is taken from a previous RANS calculation with the EB-RSM model. Using formulation (11) with mesh 1, it is noticed that the condition $\beta_0 \eta_c^{2/3} \gg 1$ is not satisfied in the centre of the channel, to recover the theoretical formulation (10), based on the Kolmogorov law. Moreover, as shown on Fig. 1, the resolved part of the Reynolds stress increases very rapidly as a function of the distance to the wall and is strongly overestimated. In the elliptic blending framework, it is proposed to blend the value of f_k near the wall ($f_k = 1$) and its theoretical value, given by Eq. (10), valid far from the wall, as

$$f_k = (1 - \alpha^p) + \alpha^p \frac{1}{\beta_0 \eta_c^{2/3}} \qquad (12)$$

Formulation (12) enables a better control of the transition RANS–LES, as shown on Fig. 1, because f_k is not only a function of the local cell size, but also of the distance to the wall, implicitly contained in α. Using the exact asymptotic behaviour at the wall of the different quantities ($k = \mathcal{O}(y^2)$, $\varepsilon = \mathcal{O}(1)$, $\alpha = \mathcal{O}(y)$, it can be shown that $p \geq 16/9$ leads to a correct asymptotic behaviour of f_k at the wall. For simplicity, p is chosen as an integer, $p = 2$.

A range of values between 2 and 20 have been tested for the C_g parameter, which enters the evaluation of β_0. Indeed, the highest frequency which can be obtained on a given mesh depends on the numerical scheme, and [10] recommends the value $C_g = 6$ for a second order CDS. For large values of C_g, $f_k = 1$ is obtained all across the channel, thus leading to a RANS solution. $C_g < 4.5$ leads to a too weak subgrid-scale dissipation and a strong overestimation of the total Reynolds stresses. In the range $[4.5, 10]$, the turbulence statistics are weakly dependent on the value of C_g. The optimal value was found to be $C_g \simeq 6.5$ ($\beta_0 = 0.20$), which is very close to the value suggested by [10].

LENGTH SCALE FOR THE WALL-BLOCKING EFFECT

In a RANS framework, the elliptic relaxation equation Eq. (6) is solved, where the length scale is given by

$$L = C_L \max\left(\frac{k^{3/2}}{\varepsilon}, L_b\right) \qquad (13)$$

where L_b is related to the Kolmogorov scale L_η by $L_b = C_\eta L_\eta$. The constants are $C_L = 0.161$ and $C_\eta = 80$.

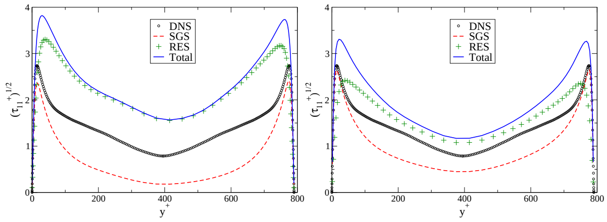

Figure 1: Influence of the form of f_k. Mesh 1, component τ_{11}, $\beta_0 = 0.20$. Profile of resolved (RES), modelled (SGS) and total stress. Left: f_k given by Eq. (11). Right: f_k given by Eq. (12).

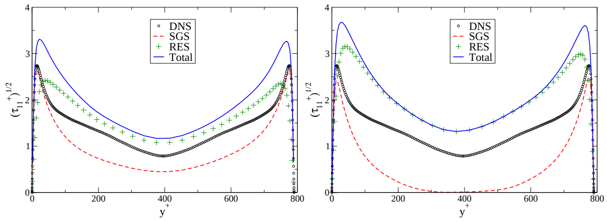

Figure 2: Influence of the value of β_0. Mesh 1, component τ_{11}, f_k given by Eq. (12). Profile of resolved (RES), modelled (SGS) and total stress. Left: $\beta_0 = 0.20$. Right: $\beta_0 = 0.60$.

As mentioned above, this length scale characterizes the distance at which the non-local kinematic blocking of the wall is felt by the non-resolved motion. In the hybrid context, the length scale of the non-resolved fluctuations is dependent on the width of the filter, and the modelling of the length scale must be consequently modified.

In order to illustrate the influence of this length scale, it is noted that the solution of Eq. (6) can be roughly approximated by

$$\alpha(y) = 1 - \exp\left(-\frac{y}{L_{\text{SGS}}}\right), \tag{14}$$

with a constant length scale, where L_{SGS} must be lower than the admissible value for a RANS computation: $0.03H$. Fig. 3 shows the influence of the blocking effect on the anisotropy by comparing the results obtained with $L_{\text{SGS}} = 0.02H$ and $0.03H$. It is seen that the decrease of L_{SGS} modifies the anisotropy, by reducing the blocking effect, i.e., the inhibition of the redistribution from τ_{11} to τ_{22}. As expected, the blocking effect only affects the subgrid scales, leaving the resolved scales unchanged.

The reduction of the length scale can be achieved by replacing the integral length scale $k^{3/2}/\varepsilon$ in Eq. (13) by the length scale characterizing the largest subgrid eddies $k_m^{3/2}/\varepsilon$, and the lower bound must be reduced by the same factor, i.e., $f_k^{3/2}$, which yields

$$L_{\text{SGS}} = C_L \max\left(\frac{k_m^{3/2}}{\varepsilon}, f_k^{3/2} L_b\right) \tag{15}$$

At the RANS limit ($f_k = 1$), Eq. (13) is recovered. Formula (15) is also compatible with the DNS limit ($f_k = 0$) because $L_{\text{SGS}} = 0$, leading to $\alpha = 1$ (see Eq. (6)), which corresponds to a vanishing of the blocking effect, as the subgrid scales vanish.

Using this formulation, Fig. 4, Fig. 5, Fig. 6 and Fig. 7 show the profile of resolved, modelled and total stresses, for the two meshes. Fig. 8 shows the profile of resolved, modelled and total kinetic energy. It can be seen that near the wall, the SGS part is dominant and decreases toward the centre of the channel, where the resolved part in turn becomes dominant. When the mesh is refined, the cutoff wave number is increased (Eq. (12)), and the balance resolved/modelled energy is modified as expected. The total energy is not perfectly constant, but varies much less than the two contributions. On the refined mesh, a quasi-DNS is performed in the centre of the channel because the modelled part is nearly zero.

The mean velocity is shown on Fig. 10, for the two meshes. Comparison is done with the DNS, a RANS computation with the EB-RSM model, and a LES with the dynamic Smagorinsky model. It appears that on the coarse grid, the present hybrid model performs much better than the Smagorinsky model, due to the fact that the cutoff is not in the inertial range. Mesh 2 is an acceptable LES mesh, and the Smagorinsky model gives good prediction. These results show one of the interests of the present approach, which gives acceptable results with a mesh coarser than a LES mesh.

For the two meshes, Fig. 9 shows the near-wall structures, as the hairpin vortices and the streaks, by positive isocontours of the Q-criterion, colored by the velocity magnitude. This figure confirms that by refining the mesh, the solution tends to a typical LES solution.

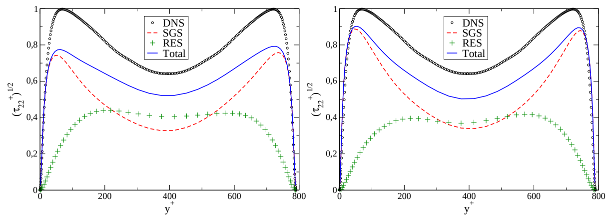

Figure 3: Influence of L_{SGS}. Mesh 1, component τ_{22}. f_k and α given by Eq. (12) and Eq. (14) and $\beta_0 = 0.20$. Profiles of resolved (RES), modelled (SGS) and total stress. Left: $L_{\text{SGS}} = 0.03H$ (RANS value). Right: $L_{\text{SGS}} = 0.02H$.

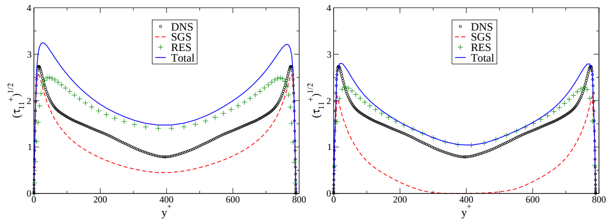

Figure 4: Profile of resolved (RES), modelled (SGS) and total stress. Component τ_{11}. Left: mesh 1. Right: mesh 2.

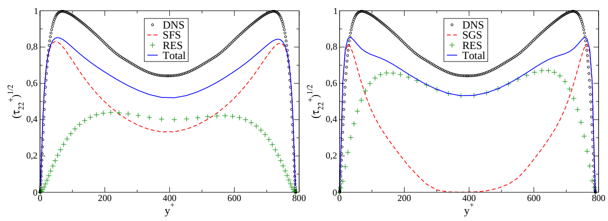

Figure 5: See caption of Fig. 4. Component τ_{22}.

MODIFICATION OF THE SLOW PART OF THE PRESSURE TERM

In the elliptic blending model, the pressure term ϕ_{ij} is decomposed into a near-wall contribution ϕ_{ij}^w and a "homogeneous" contribution ϕ_{ij}^h. The latter, given here by the SSG model [23], can be decomposed into a rapid part $\phi_{ij}^{h,r}$, depending directly on the mean velocity, and a slow part $\phi_{ij}^{h,s}$

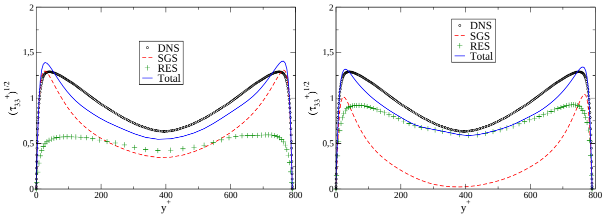

Figure 6: See caption of Fig. 4. Component τ_{33}.

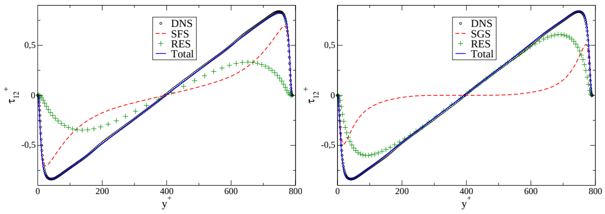

Figure 7: See caption of Fig. 4. Component τ_{12}.

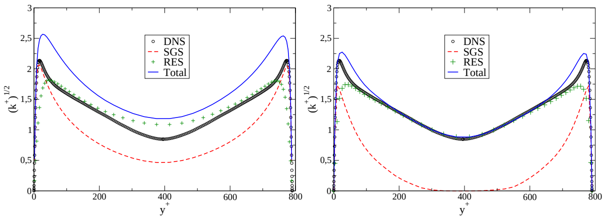

Figure 8: See caption of Fig. 4. Turbulent kinetic energy.

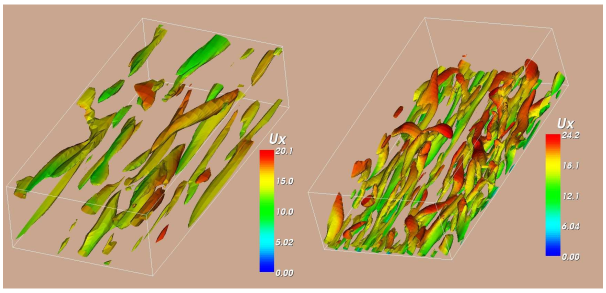

Figure 9: Isocontours of Q-criterion colored by resolved velocity. Left: mesh 1. Right: mesh 2, bottom wall.

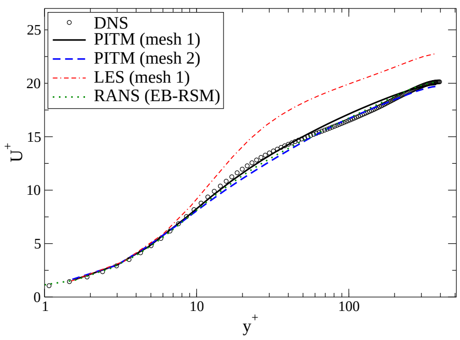

Figure 10: Mean velocity profile. Comparison with RANS (EB-RSM), DNS and LES calculations (Dynamic Smagorinsky model).

which effect is to force the turbulence to return to isotropy. In the hybrid context, following [4] and [18], to take into account the fact that the small scales return to isotropy faster than the large scales, an empirical parameter f_{SGS} is introduced as

$$\phi_{ij}^{h} = f_{SGS}\,\phi_{ij}^{h,s} + \phi_{ij}^{h,r} \tag{16}$$

The parameter f_{SGS} must be an increasing function of the dimensionless cutoff wave-number η_c. To be consistent with the RANS limit, it is necessary to have $\lim_{\eta_c \to 0} f_{SGS} = 1$. Similarly to Eq. (12), we propose

$$f_{SGS} = (1-\alpha^b) + \alpha^b \frac{\gamma \eta_c^2}{1+\eta_c^2} \tag{17}$$

where $\gamma = 1.5$, following [4]. In order to have a real effect on the anisotropy, it was found that the value of b must be less than one, and $b = 0.5$ is chosen here. At the wall, the RANS limit is recovered since $\alpha = 0$. At the DNS limit ($\eta_c \to \infty$), far away from the wall ($\alpha = 1$), $f_{SGS} \to \gamma$, meaning that the small scales return to isotropy faster than the large scales by a factor γ. As shown in Fig. 11, the value of the peak of τ_{22} is improved, without really reducing the overestimation of the peak of τ_{11}, compared to the case where the parameter f_{SGS} is not taken into account (Figs. 4 and 5). Surprisingly, the main effect of the modification is to modify the balance between resolved and modelled energy, in particular at the centre of the channel, as shown by Fig. 12. Actually, this behaviour can be explained by the fact that the parameter f_{SGS}, by forcing turbulence toward isotropy, tends to decrease the amplitude of the shear stress $-\tau_{12}$, and, as a consequence, the production of subgrid energy goes to zero. Since, on the other hand, the effect on the anisotropy of the normal stresses is marginal, the use of this modification of the return to isotropy is not recommended.

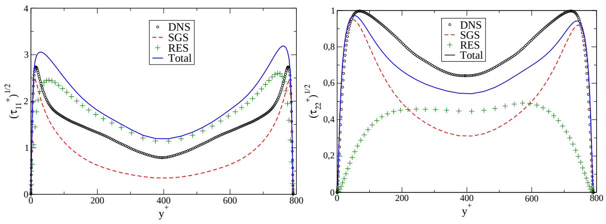

Figure 11: Influence of the parameter f_{SGS}. Mesh 1, f_k and L_{SGS} given by Eq. (12) and Eq. (15), $\beta_0 = 0.20$. Profile of resolved (RES), modelled (SGS) and total stress. Left: component τ_{11}. Right: component τ_{22}.

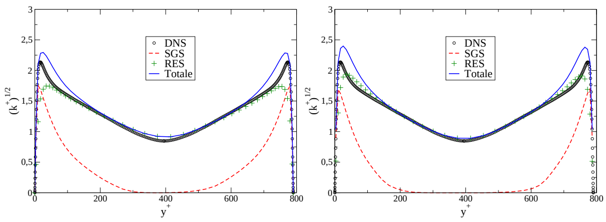

Figure 12: Influence of the parameter f_{SGS}. Mesh 2, f_k and L_{SGS} given by Eq. (12) and Eq. (15), $\beta_0 = 0.20$. Profile of resolved (RES), modelled (SGS) and total fluctuating kinetic energy. Left: without parameter f_{SGS}. Right: with parameter f_{SGS}.

CONCLUSIONS

A new hybrid RANS–LES model, based on transport equations for the subgrid stresses, and the elliptic blending method to account for the non-local kinematic blocking due to the wall, has been developed. The derivation is made in the framework of the Partially Integrated Transport Model (PITM) proposed by [19] and [4]. The purpose of such a model is to obtain the unsteady characteristics of the flow at a cost lower than LES, by going to a RANS computation in the near-wall region, and also by making the use of coarse meshes (compared to LES meshes) possible. Therefore, the cutoff can be located in the productive zone of the spectrum, and, therefore, the complex production and redistribution mechanisms must be reproduced. For this purpose, the elliptic blending hybrid model is based on transport equations for the subgrid scale tensor and the dissipation rate. The wall blocking effect is reproduced by using an additional elliptic relaxation equation for the blending function α, which drives the transition of the subgrid-scale pressure term from a near-wall behaviour to a quasi-homogeneous behaviour. A new form of the parameter f_k, which provides the model with the target ratio modelled/total kinetic energy, is proposed to better control the RANS–LES transition in the near-wall region, and is carefully calibrated in the channel flow at $Re_\tau = 395$. A new formulation of the length scale for the elliptic relaxation equation is also proposed, in order to account for the fact that the kinematic blocking must be modelled only for the subgrid-scales. The results in channel flow are very encouraging in terms of mean flow and turbulence statistics, and show that the present approach indeed gives better results than a LES with the dynamic Smagorinsky model when the mesh is coarsen.

∗ References

[1] F. Archambeau, N. Méchitoua, and M. Sakiz. Code Saturne: A finite volume code for the computation of turbulent incompressible flows - Industrial applications. *Int. J. on Finite Volume, Electronical edition: http://averoes.math.univ-paris13.fr/html*, ISSN 1634(0655), 2004.

[2] P. Batten, U. Goldberg, and S. Chakravarthy. LNS-An approach towards embedded LES. AIAA paper 0427, 40th Aerospace Sciences Meeting and Exhibit, Reno, Nevada, 2002.

[3] D. Borello, K. Hanjalić, and F. Rispoli. Prediction of cascade flows with innovative second-moment closure. *J. Fluids Eng.*, 127(6):1059–1070, 2005.

[4] B. Chaouat and R. Schiestel. A new partially integrated transport model for subgrid-scale stresses and dissipation rate for turbulent developping flows. *Phys. Fluids*, 17:1–19, 2005.

[5] S.-K. Choi and S.-O. Kim. Computation of a turbulent natural convection in a rectangular cavity with the elliptic-blending second-moment closure. *International Communications in Heat and Mass Transfer*, 33(10):1217–1224, 2006.

[6] B. J. Daly and F. H. Harlow. Transport equations in turbulence. *Phys. Fluids*, 13:2634–2649, 1970.

[7] P. A. Durbin. Near-wall turbulence closure modeling without “damping functions”. *Theoret. Comput. Fluid Dynamics*, 3:1–13, 1991.

[8] P. A. Durbin. A Reynolds stress model for near-wall turbulence. *J. Fluid Mech.*, 249:465–498, 1993.

[9] M. Germano. Turbulence: the filtering approach. *J. Fluid Mech.*, 238:325–336, 1992.

[10] S. Ghosal. An analysis of numerical errors in large eddy simulations of turbulence. *J. Comput. Physics*, 125:187–206, 1996.

[11] S. S. Girimaji. Partially-Averaged Navier-Stokes model for turbulence: a Reynolds-Averaged Navier-Stokes to Direct Numerical Simulation bridging method. *J. Appl. Mech.*, 73:413–421, 2006.

[12] Y. Hoarau, R. Perrin, M. Braza, D. Ruiz, and G. Tzabiras. Advances in turbulence modelling for unsteady flows. In *Flomania - A European initiative on flow physics modelling*, volume 94, pages 85–88. W. Haase, B. Aupoix, U. Bunge and D. Schwamborn (Editors), 2006.

[13] G. Iaccarino, A. Ooi, P. A. Durbin, and M. Behnia. Reynolds averaged simulation of unsteady seperated flow. *Int. J. Heat & Fluid Flow*, 24:147–156, 2003.

[14] R. Manceau. An improved version of the Elliptic Blending Model. Application to non-rotating and rotating channel flows. In *Proc. 4th Int. Symp. Turb. Shear Flow Phenomena, Williamsburg, Virginia, USA*, 2005.

[15] R. Manceau and K. Hanjalić. Elliptic Blending Model: a new near-wall Reynolds-stress turbulence closure. *Phys. Fluids*, 14(2):744–754, 2002.

[16] F. R. Menter and Y. Egorov. SAS turbulence modelling of technical flows. In *Proc. 6th Int. ERCOFTAC Workshop on Direct and Large-Eddy Simulation, Poitiers, France*, volume 10, pages 687–694, 2005.

[17] R. D. Moser, J. Kim, and N. N. Mansour. Direct numerical simulation of turbulent channel flow up to $Re_\tau = 590$. *Phys. Fluids*, 11(4):943–945, 1999.

[18] R. Schiestel. Studying turbulence using numerical simulation databases. In *Proc. of the Summer Program*, pages 95–108. Center for Turbulence Research, Stanford Univ., 1987.

[19] R. Schiestel and A. Dejoan. Towards a new partially integrated transport model for coarse grid and unsteady turbulent flow simulations. *Theoret. Comput. Fluid Dynamics*, 18:443–468, 2005.

[20] J. K. Shin, K. H. Chun, and Y. D. Choi. Refinement of a second moment closure by the elliptic blending equation and its application to turbulent rotating channel flows. *J. Turbulence*, 4(030):1–22, 2003.

[21] P. R. Spalart. Strategies for turbulence modelling and simulations. *Int. J. Heat & Fluid Flow*, 21:252–263, 2000.

[22] C. G. Speziale. Turbulence modeling for time-dependent RANS and VLES: a review. *AIAA J.*, 36(2):173, 1998.

[23] C. G. Speziale, S. Sarkar, and T. B. Gatski. Modeling the pressure-strain correlation of turbulence: an invariant dynamical system approach. *J. Fluid Mech.*, 227:245–272, 1991.

[24] L. Thielen, K. Hanjalić, H. Jonker, and R. Manceau. Predictions of flow and heat transfer in multiple impinging jets with an elliptic-blending second-moment closure. *Int. J. Heat & Mass Transfer*, 48(8):1583–1598, 2005.

[25] V. Viti, G. Huang, and P. Bradshaw. Implementation and validation of recent stress-transport turbulence models: the need for standardized procedures. In *Proc. 43rd AIAA Aerospace Sciences Meeting and Exhibit, Reno, Nevada, USA*, 2005.